water

MDPI

Article

The Irrigation Cooling Effect as a Climate Regulation Service of Agroecosystems

José Antonio Albaladejo-García [1,*], Francisco Alcon [2] and José Miguel Martínez-Paz [1]

[1] Applied Economics Department, Faculty of Economics, University of Murcia, Campus de Espinardo, 30100 Murcia, Spain; jmpaz@um.es
[2] Business Economics Department, ETSIA, Polytechnic University of Cartagena, Paseo Alfonso XIII, 48, 30203 Cartagena, Spain; francisco.alcon@upct.es
* Correspondence: joseantonio.albaladejo@um.es

Received: 5 May 2020; Accepted: 27 May 2020; Published: 29 May 2020

Abstract: Agroecosystems provide a range of benefits to society and the economy, which we call ecosystem services (ES). These services can be evaluated on the basis of environmental and socioeconomic indicators. The irrigation cooling effect (ICE), given its influence on the land surface temperature (LST), is an indicator of climate regulation services from agroecosystems. In this context, the objective of this study is to quantify the ICE in agroecosystems at the local scale. The agroecosystem of citrus cultivation in Campo de Cartagena (Murcia, Spain) is used as a case study. Once the LST was retrieved by remote sensing images for 216 plots, multivariate regression methods were used to identify the factors that explain ICE. The use of a geographically weighted regression (GWR) model is proposed, instead of ordinary least squares, as it offsets the spatial dependence and gives a better fit. The GWR explains 78% of the variability in the LST, by means of three variables: the vegetation index, the water index of the crop, and the altitude. Thus, the effects of the change in land use on the LST due to restrictions on the availability of water (up to 1.22 °C higher for rain-fed crops) are estimated. The trade-offs between ICE and the other ES are investigated by using the irrigation water required to reduce the temperature. This work shows the magnitude of the climate regulation service generated by irrigated citrus and enables its quantification in agroecosystems with similar characteristics.

Keywords: ecosystem services; GIS; irrigated agriculture; Landsat; land surface temperature; water

1. Introduction

The main function of agroecosystems is traditional food and fiber production. However, other goods and services are offered by these systems, which are called ecosystem services (ES) [1]. These services can be defined as the contributions of an ecosystem to human wellbeing, which are generally classified into provisioning, support, regulation, and cultural services [2]. ES provide a framework to identify and analyze all agricultural outputs [1]. Nevertheless, not all ES contributions are positive, as there are also the so-called ecosystem disservices (EDS). EDS can be defined as the ecosystem-generated functions, processes, and attributes which result in perceived or actual negative impacts on human wellbeing [3]. In agroecosystems, there are often trade-offs between ES and EDS. For example, an increase in food production requires a greater demand for water [4]. These trade-offs become even more important in semi-arid environments, where there is water scarcity affecting the ES supply of agroecosystems [5]. Therefore, it is necessary to know the ES and EDS derived from the irrigation of semi-arid agroecosystems [6,7]. Thus, water consumption will be an EDS in these areas; however, at the same time, it will produce an ES by allowing, among others, the regulation of temperature extremes [8].

Among the regulation ES, agroecosystems may provide soil erosion control, flood control, crop pollination, or climate regulation [9,10]. These services facilitate the regulation and preservation of vital ecosystem functions that enhance health and population growth, as well as imply relationships between the biotic and abiotic elements of ecosystems [10]. In this paper, climate regulation is the ES under study. This ES has a role in regulating processes related to the chemical composition of the atmosphere, rainfall, air quality, the greenhouse effect, and the moderation of extreme temperatures, among others [9], and has acquired a special relevance in the current context of climate change.

The vegetation cooling effect is one of the indicators related to climate regulation ES [2], also known as "local and regional climate regulation" in the CICES classification system [4]. This climate phenomenon contributes to temperature control by decreasing the intensity of extreme temperature values [11]. Climate regulation is generated by the oasis effect of water evaporation, photosynthesis, and the provision of shade, which has an influence on convective and evapotranspiration processes [12]. Thus, irrigated agriculture generates an irrigation cooling effect (ICE) [13]. Like other climatic phenomena at the local scale, such as the urban heat island [14], it is affected by changes in land use and/or land cover [15].

An indicator of climate regulation ES, such as ICE, can be used to show the ability of agricultural ecosystems to modify the temperature and thus to contribute to the mitigation of one of the effects of climate change [10], especially in warm-climate areas [4]. In this regard, agroecosystem functions such as ICE can provide socioeconomic benefits to the population [2]. The study of ICE at the spatial level promotes the incorporation of this climatic phenomena into ES maps [1]. Furthermore, spatial analysis allows for the determination of the factors that explain its territorial distribution. This is very useful to guide and inform the formulation and development of policies related to the provision of these services [16].

The European Union has recognized the fundamental role played by ecosystems in mitigating climate change [17], considering the ES of climate regulation to be essential. The Common Agricultural Policy considers the improvement and preservation of agroecosystems as one of its six basic priorities for rural development [18], one of its aims being reducing the impact of climate change at the local scale [15,17].

The study of climate regulation ES has mainly focused on carbon sequestration and the reduction of the urban heat island by vegetation and agriculture [19–24]. Meanwhile, the specific analysis of the ICE has been fundamentally addressed at the global [25–27] or regional [11,28–30] level, based on climate models. Nevertheless, climate models, given their spatial resolution, lose precision in the modelling of local effects and provide little precision in the characterization of the ICE at the local or regional level [31].

For this reason, in order to study the ICE in specific ecosystems (which provides local ES), remote sensing techniques are often used. The evaluation of the ICE is typically carried out on the basis of the land surface temperature (LST) retrieved from satellite images [32]. The LST is not only a determining factor in the study of the climate, as it can modify the air temperature [24], but also a good indicator of the energy balance at the land surface. This approach has been used for agroecosystems: for example, in the study of the role of irrigated crops in the cooling of urban areas around the Yangtze river (China) [33], in irrigated agriculture across China [34], and in the evaluation of the ability of trees in agricultural ecosystems to reduce the temperature in the dehesa-type production system in Spain [35].

In order to determine the factors that influence the reduction of the LST and, therefore, the provision of climate regulation ES, multivariate regression modelling has been used [36]. The spatial nature of the data means that the use of conventional econometric techniques, such as ordinary least squares (OLS), may not be adequate when the residuals present problems of non-normality or spatial dependence [37]. When spatial dependence is present, the use of the local geographically weighted regression (GWR) has been proposed [38]. The use of this type of model has become increasingly frequent in studies with spatial data [38–40]. In fact, the use of GWR models has been previously used to study the relationships

between the LST and its influencing factors in the context of the urban heat island [40–44] but not in the generation of the ICE.

In this context, this paper proposes the quantification of the ICE in agroecosystems at the local scale, through the study of spatial patterns of LST reduction produced in irrigated agriculture. OLS and GWR models are used to test which method allows for its correct quantification [40–44].

In addition to the existence of a cooling effect in irrigated agroecosystems in the study area, the factors determining the ICE are studied [36]. To this end, multivariate regression techniques are used, paying special attention to the character of the sample. Modelling makes it possible to quantify the effect of changes in land-use and land-cover on this climate phenomenon and, in short, on the ES of climate regulation. This quantification is important to obtain temperature data that allows the subsequent joint valuation of ES in these agroecosystems [16,17].

In order to achieve this objective, irrigated citrus fruit crops in an agricultural region of the Western Mediterranean with limited water resources are studied. In the last 40 years, the area has undergone a profound change in land use, moving from dry to irrigated systems, especially in the case of citrus. This has also happened in other areas of the Mediterranean basin [45], Florida [46], and California [47], which makes this case study of interest beyond the local scale.

2. Materials and Methods

2.1. Study Area

The agricultural region of Campo de Cartagena, located in the Region of Murcia (Southeastern Spain; see Figure 1), is affected by a semi-arid climate, with an average annual temperature and rainfall of 18 °C and 350 mm, respectively. The use of water resources from the Tagus–Segura transfer (122 hm^3/year) and groundwater (89.44 hm^3/year) [48] has led to this region undergoing, in recent decades, a very important change in both land-use and current production orientations [49]. Thus, this region increased its irrigated agricultural area by 57.13% over the period of 1984–2016. Currently, there is a total of 47,430 ha of irrigated land, while rain-fed land has declined to 13,896 ha [50]. Of the irrigated land in the study area, there is a notable extension (8000 ha) dedicated to citrus cultivation (lemon, orange, mandarin, and grapefruit).

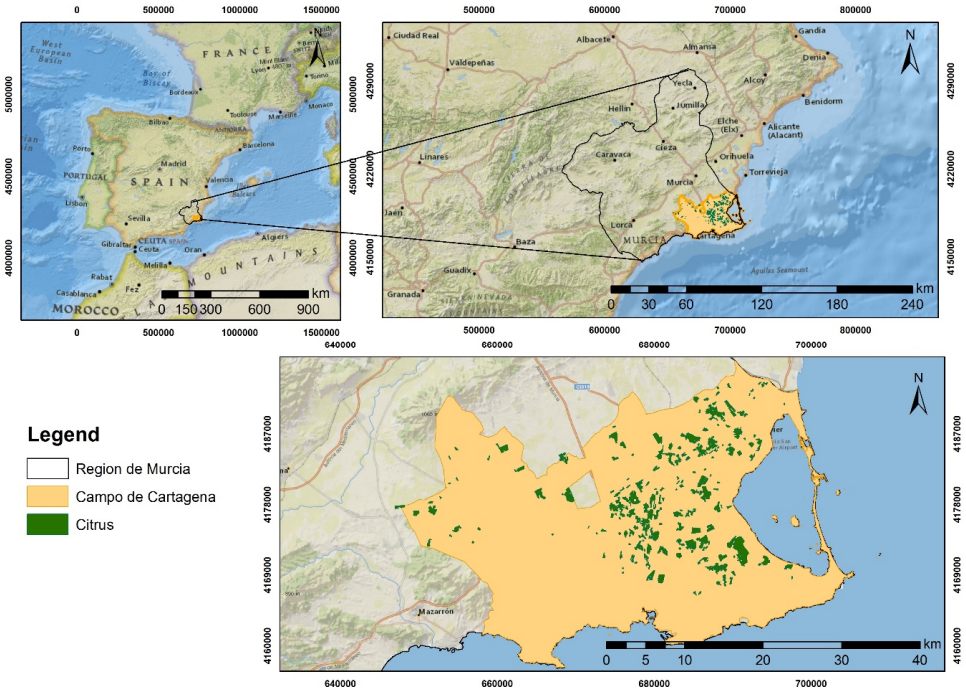

Figure 1. The study area.

2.2. Methodology

In order to quantify the ICE through the study of spatial LST patterns, information was gathered from 216 citrus plots registered in Campo de Cartagena in 2016 from the Information System on Land Occupancy in Spain (SIOSE) [51]. These plots have a drip irrigation system and an average area of 3.10 ha. All plots had the same average water supply managed by Irrigation Communities. For each plot, both the LST and the different factors influencing it were measured. The factors which could explain the variability in LST were chosen through a review of previous related work [33,52]: air temperature (Tair), Normalized Difference Vegetation Index (NDVI), Normalized Difference Water Index (NDWI), distance to the coast (Dist-coast), altitude, slope, and dominant orientation. The techniques used for factor estimations were remote sensing and the use of spatial databases with GIS tools.

This work complements the study of Zabala et al. [8], which attempted to identify all the ES of Mediterranean irrigated agriculture. One of the ES identified as relevant was climate regulation. Considering water consumption as a limiting factor, changes in the supply of this ES can be observed. These changes will occur when moving from an irrigated to a rain-fed agroecosystem, as a result of water scarcity in the area. However, climate regulation ES was not quantified previously, this work being the first to obtain climate regulation ES by retrieving LST from satellite images. In fact, local climate regulation ES is the ES least commonly quantified in agroecosystems. In addition, water consumption was also taken into account, with an analysis of the trade-offs with other ES.

2.2.1. Land Surface Temperature retrieval and its influencing factors

The LST (°C) was retrieved from the information contained in satellite images of the Landsat 8-OLI-TIRS remote sensor of the United Stated Geological Survey (USGS). The image under consideration has multispectral bands with a spatial resolution of 30 m (in 100 m thermal bands) and the coordinate system ETRS89. The image was captured under clear conditions (0% cloudy) in summer (27 July 2016 at 10:44:01 a.m.) and was corrected radiometrically, passing values from Digital Numbers to top-of-atmosphere values. A single-satellite image was selected, in summer dates, as is usual in other studies [14,26,44,53–55], due to the great impact that irrigation has on extreme temperatures and the scarce influence on other seasons of the year. Thus, the use of a single-satellite image was intended to carry out a spatial comparison between land uses, rather than a temporal analysis.

For the retrieval of the LST, the Chander and Markham technique [56] was used. This technique was proposed by the USGS [57], does not require climatic variables, and is generally used to retrieve this variable from satellite information using the expression:

$$\mathrm{LST} = \frac{\mathrm{T_B}}{1 + \mathrm{W} \times \left(\frac{\mathrm{T_B}}{\mathrm{P}}\right) \times \ln(\mathrm{LSE})}, \quad (1)$$

where T_B is the brightness temperature, W is the wavelength of emitted radiation, P is a constant (14,380), and LSE is the emissivity correction factor proposed by Sobrino [58]. The first two variables are provided by the image used.

To explain the LST factors, information was obtained from the variables NDVI and NDWI, obtained from the same satellite image:

$$\mathrm{NDVI} = \frac{\mathrm{NIR} - \mathrm{R}}{\mathrm{NIR} + \mathrm{R}} \quad (2)$$

$$\mathrm{NDWI} = \frac{\mathrm{NIR} - \mathrm{SWIR}}{\mathrm{NIR} + \mathrm{SWIR}} \quad (3)$$

where NIR is near-infrared (band 5), R is visible red (band 4), and SWIR is short wavelength-infrared (band 6). The combination of these bands allowed us to measure the intensity of the green vegetation and the amount of water it contains [59]. The values of these indices range from −1 to 1; the higher the value, the healthier and denser the vegetation. Differences in values are determined by the irrigation

of the area, after confirming the absence of rainfall days prior to the satellite image selected. For the previous month, no rain events (0 mm) occurred in the study area [60].

Average Tair in °C was based on the interpolation of Tair values from meteorological stations in the study area [60].

Average altitude (m), average slope (°), and orientations (−1: shaded spot, 0: flat, 1: sunny spot) were obtained from the digital elevation model [61]. Given the different shapes of the plots, the averages of these plots were selected to obtain the average altitudes and slopes. In the case of the orientations, the most frequent orientation value of the plot was selected.

Average Dist-coast of the irrigated citrus plots (km) [51]; the study region is adjacent to the Mediterranean Sea, which is largely affected by the sea currents and wind. For this study, Dist-coast was considered as a proxy for the oceanic and atmospheric states [43].

The information used in this study, as described in Table A1, is fully recorded in a data repository [62], where data from the variables used in the multiple linear regression models for the 216 citrus plots are shown.

2.2.2. Spatial Regression Model

The OLS method is the most frequently used method to estimate a linear regression model. This is due to its simplicity and the optimal character of the estimated parameters for cross-sectional data sets. This technique has been used to study samples distributed in space, assuming that the relationships are spatially constant [41]. A global regression model is expressed as:

$$y_i = \beta_0 + \beta_1 x_{i1} + \cdots + \beta_n x_{in} + \varepsilon_i \quad (4)$$

where, for each observation i, y_i is the dependent variable, x_{i1} to x_{in} are the independent variables, β_0 is the intercept, β_1 to β_n are the estimated coefficients, and ε_i is the sampling error, these parameters being invariant.

Nevertheless, OLS estimation with spatial data often fails to comply with one of the basic hypotheses of this technique, such as the independence of residuals. The residuals are spatially autocorrelated due to the spatial dependence of the study variable. This leads to OLS estimators being inefficient, and hence, the model suffers from poor specification.

To determine the degree of spatial concentration or dispersion of the data, an indicator of spatial autocorrelation is applied, such as Moran's I index [63,64]. In the presence of spatial autocorrelation, it is necessary to apply a technique specifically designed to treat and model it, such as GWR [38–42].

The GWR technique makes it possible to estimate multivariate regression models by incorporating the spatial dependence of the data. The GWR model makes the estimates of coefficients a function of the location and quantifies them separately and independently for each sample unit, passing from a global analysis to a local one [63]. The GWR model can be expressed as:

$$y_i = \beta_0(\mu_i, v_i) + \beta_1(\mu_i, v_i)x_{i1} + \cdots + \beta_n(\mu_i, v_i)x_{in} + \varepsilon_i \quad (5)$$

where (μ_i, v_i) indicates the co-ordinates of each observation (which act as weights), and $\beta(\mu_i, v_i)$ are the coefficients of the model (which vary with the location). Thus, for each observation, the estimate provides both a value for each coefficient and a measure of the adjustment, allowing the local variation and the effects of the variables to be studied individually.

A weighting scheme known as adaptive Gaussian Kernel [64] was used in the allocation of GWR model weights. It assigns a higher weight to the closest observations, which is zero if the distance between the two observations exceeds the bandwidth distance, calculated for each case by cross-validation [62].

In order to compare the quality of the models, the corrected Akaike information criterion (AICc) and the corrected determination coefficient (R^2c) [37,41,64] were used. In addition, for prediction

purposes, the root mean square error (RMSE) was used to compare the measure of performance of the final models [65].

3. Results

3.1. Spatial Distribution of the LST and its Influencing Factors

Firstly, a satellite image was selected from the Landsat 8 remote sensor on 27 July 2016. The image corresponds to the period in which the highest temperatures of the year occurred in the study area [48]. From this satellite image, the LST was retrieved. Figure 2a shows the spatial distribution of the LST, with maxima in the central-western zone and minima in the east and south. This distribution is consistent with that of the agricultural uses by comparing LST from irrigated and dry lands (Figure 2b). On 27 July 2016, more than one-third of the study area was above 35 °C, while the 216 irrigated citrus plots in the agricultural zone (Figure 2c) had an average LST of 32.47 °C.

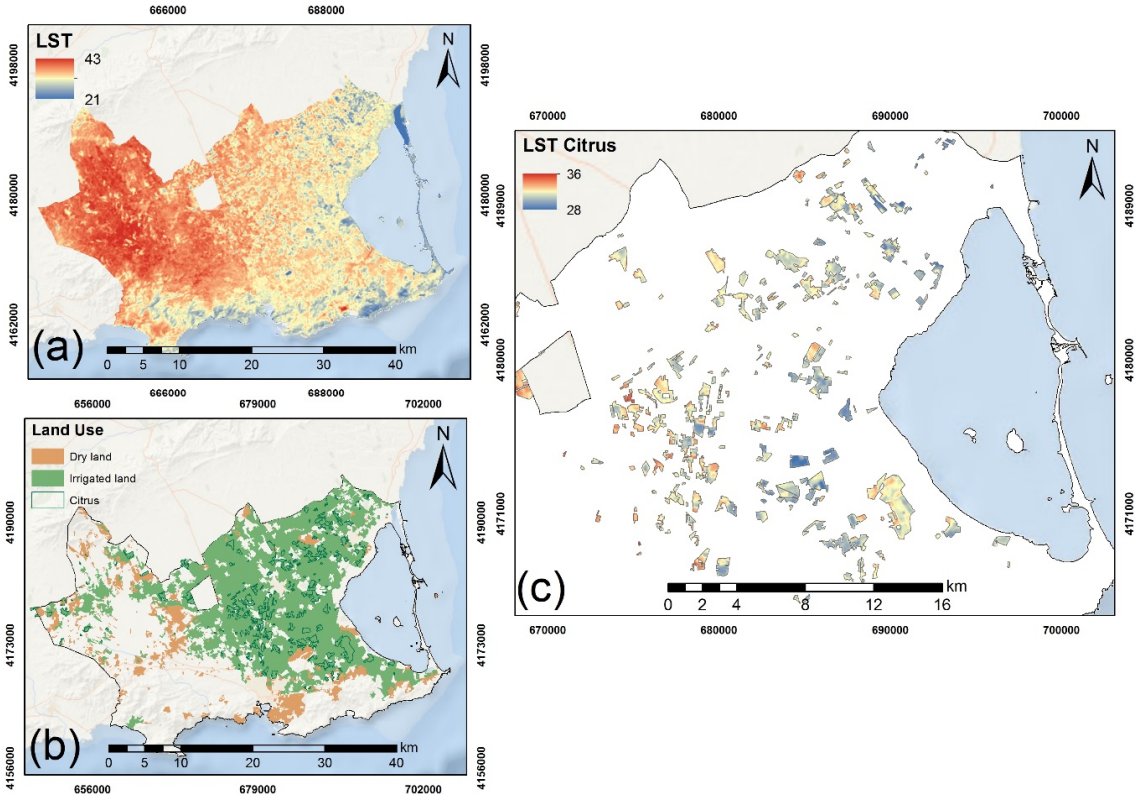

Figure 2. Land surface temperature (LST; °C) retrieved at the regional scale (**a**); agricultural land uses (**b**); and LST (°C) in citrus plots (**c**) at Campo de Cartagena. Data were obtained following [51, 56], respectively.

We analyzed seven factors, whose descriptive statistics and spatial distributions are shown in Table A1 and Figure A1, respectively. The citrus plots had mean altitudes and slopes of 58.56 m and 1.50°, respectively. The plots with the highest altitudes and slopes were located in the western and southern parts of the study area. Of the plots, 75.25% had a flat orientation, the average Dist-coast was 9.65 km (the plots furthest from the sea were 31 km away and the nearest were 0.5 km away), and the average Tair was 25.88 °C (with minimum and maximum temperatures of 24.88 and 26.627 °C, respectively). From the spectral indices, an average NDVI of 0.34 and an average NDWI of 0.07 were obtained (with maximum values up to 0.67 and 0.31, respectively).

3.2. LST Models

Based on the factors selected to explain the ICE, a multiple linear regression model was first fitted using an OLS procedure. Using the backward stepwise selection procedure, the model was found to have three significant factors: NDVI, NDWI, and the distance of the plots to the coast (Dist-coast). This specification explained practically three-quarters of the LST variability in irrigated citrus plots (R^2c = 0.722), without problems of multicollinearity or stationarity [66] (Table 1).

Table 1. Results for the first ordinary least squares (OLS) and geographically weighted regression (GWR) models.

Variables	OLS-1 Model		GWR-1 Model			
	Coefficients	*p*-Value	Minimum	Mean	Maximum	Standard Deviation
Intercept	32.824	0.000	31.687	33.146	36.727	0.934
NDVI	−2.881	0.001	−5.357	−2.968	−1.060	0.698
NDWI	−7.010	0.000	−10.426	−6.653	−1.294	1.524
Dist-coast	0.113	0.000	−0.066	0.099	0.187	0.045
Observations	216			216		
R^2c	0.722			0.763		
AICc	517.163			493.895		
Moran´s I index	0.227			0.037		
Moran´s I index Prob (*P*-value)	0.000			0.072		
Pattern	Clustered			Clustered		

Table 1 presents the results of the first GWR model, with improved adjustment relative to the OLS model (higher R^2c and lower AICc). Although the use of this model diminished the spatial autocorrelation, it was not completely corrected and there was still a spatial pattern clustered in the residuals, indicating that the model was mis-specified.

Given that Dist-coast, one of the three significant variables, itself had a spatial pattern of clustering (Moran´s I index = 0.695, *P*-value = 0.000), the estimation was performed again with the two remaining factors, both by OLS (OLS-2) and by GWR (GWR-2), obtaining the results presented in Table 2. The OLS-2 model had a worse fit (R^2c = 0.544) and continued to show spatial autocorrelation, while the GWR-2 model improved the fit (R^2c = 0.77, AICc = 490.11) and neutralized the spatial dependence effect (random pattern).

Table 2. Results for the second OLS and GWR regression models.

Variables	OLS-2 Model		GWR-2 Model			
	Coefficients	*p*-Value	Minimum	Mean	Maximum	Standard Deviation
Intercept	34.337	0.000	32.680	33.907	35.163	0.703
NDVI	−4.364	0.000	−7.570	−2.997	1.702	1.990
NDWI	−6.144	0.000	−12.799	−6.514	−1.058	2.975
Observations	216			216		
R^2c	0.544			0.769		
AICc	622.896			490.107		
Moran´s I index	0.227			0.005		
Moran´s I index Prob (*P*-value)	0.000			0.992		
Pattern	Clustered			Clustered		

The results show that the Dist-coast variable caused a clustered spatial distribution of the residuals from the local model. Therefore, it was eliminated from the set of seven initial factors considered. Finally, the models were estimated with the remaining six, obtaining the results shown in Table 3.

Table 3. Results for the third OLS and GWR regression models.

Variables	OLS-3 Model		GWR-3 Model			
	Coefficients	***p*-Value**	**Minimum**	**Mean**	**Maximum**	**Standard Deviation**
Intercept	33.334	0.000	31.356	33.007	34.404	0.697
NDVI	−3.217	0.001	−6.264	−2.145	0.962	1.614
NDWI	−6.686	0.000	−11.955	−7.775	−2.317	2.366
Altitude	0.011	0.000	0.004	0.015	0.0456	0.010
Observations	216			216		
R^2c	0.683			0.781		
AICc	544.910			480.171		
Moran´s I index	0.265			−0.006		
Moran´s I index Prob (*P*-value)	0.000			0.936		
Pattern	Clustered			Clustered		
RMSE	0.818			0.726		

In this model, both OLS and GWR estimation show three significant explanatory factors: the two already present in the previous specifications—NDVI and NDWI—plus the altitude above sea level of the plot (Altitude). While the problems of spatial autocorrelation persisted in the OLS estimation, the residuals had a random pattern in the GWR estimation. In turn, the GWR model showed the best fit (R^2c = 0.78, AICc = 480.17) of all the models presented.

The analysis of variance (ANOVA) of the GWR model (Table 4) confirmed that the GWR specification showed the best fit, where there was a significant reduction in the magnitude of the residuals. In addition, lower RMSE values in the GWR model indicate smaller differences between predicted and observed values than in the OLS model. It should be noted that non-linear specifications were tested, and the interactions between factors were not significant.

Table 4. ANOVA of the improvement in model fit of GWR over OLS.

Source	Sum of Squares	Degrees of Freedom	Mean Square	F	*p*-Value
OLS Residuals	150.282	3	-	-	-
GWR improvement	57.598	27.385	2.103	-	-
GWR Residuals	92.684	185.615	0.499	4.214	0.000

Therefore, the GWR model met all the criteria of econometric validation and explained 78% of the variance of the LST, based on three variables. Hence, a higher NDVI or NDWI or lower altitude reduces the surface temperature of the citrus plots. Based on the mean values of the model coefficients, each additional NDVI point reduced the LST by 2.15 °C, each NDWI point reduced the LST by 7.78 °C, and each 100 m of altitude above sea level increased the temperature of the plots by 1.50 °C.

The GWR model also makes it possible to evaluate the changes in local relationships between the LST and its explanatory factors at all points in the sample. By studying the local fit for each of the citrus plots of the study area, local R^2 values of the GWR-3 model were obtained (as shown in Figure 3a). Figure 3a also shows that the plots closer to the coast, especially to the northeast, explained better the variation in the modelled LST. In addition, the variation in the local regression coefficients of the GWR-3 model (Figure 3b–e) reflected the spatial heterogeneity of the adjustments. Meanwhile, the representation of the standard residuals of the GWR-3 model (Figure 3f) confirmed the random spatial pattern.

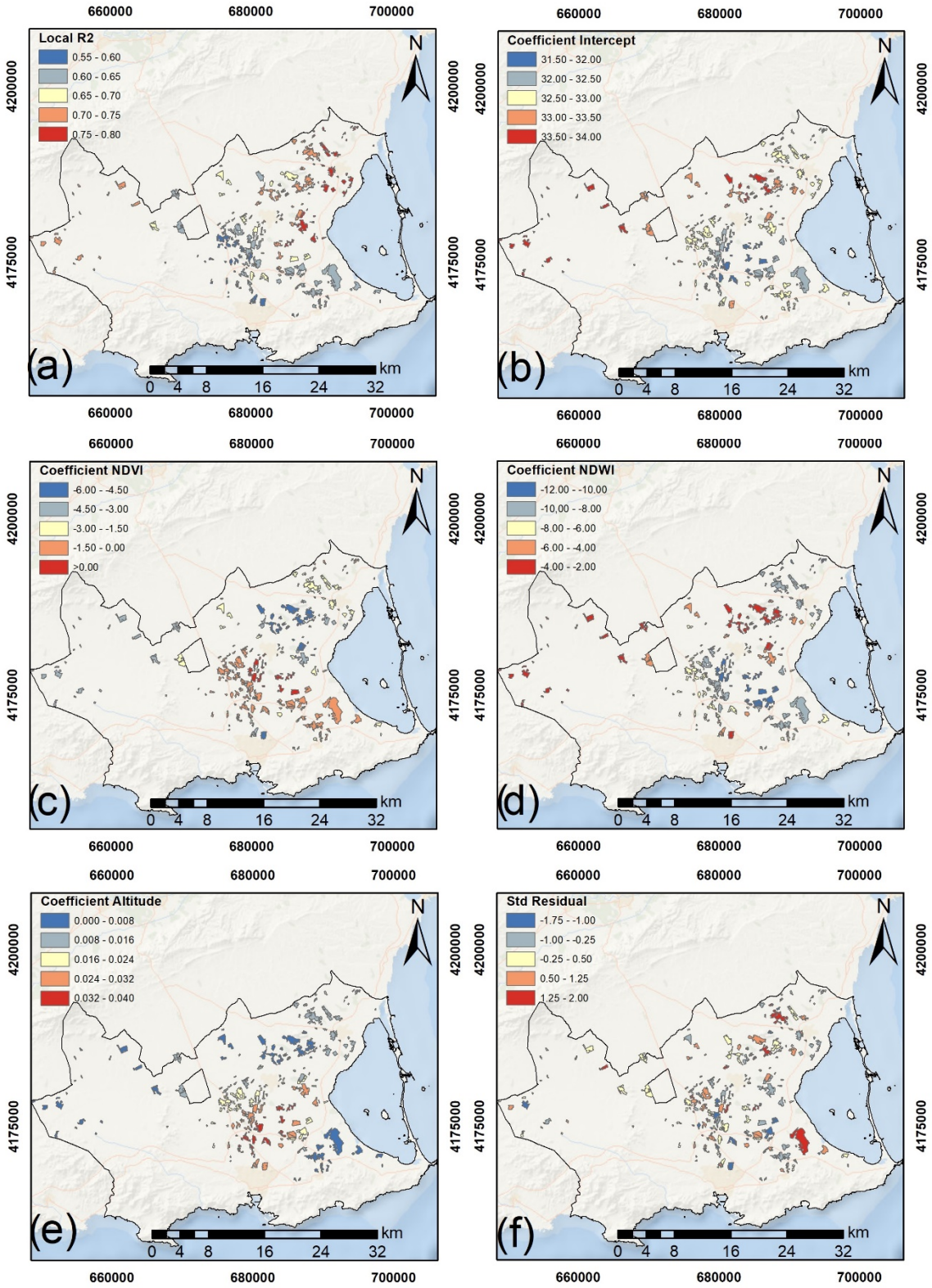

Figure 3. Spatial distribution of Local R^2 (**a**); local coefficients in the GWR model: the intercept (**b**); Normalized Difference Vegetation Index (NDVI) (**c**); Normalized Difference Water Index (NDWI) (**d**); Altitude (**e**); and standard residuals (**f**).

3.3. LST Predictions based on Changes in Land Use and Land Cover

The structural utility of the GWR-3 model has been proved. This model allows us to identify the factors that explain the ICE of the agricultural system. In addition, this model has a predictive utility that allows determination of the effects of land-use changes on target ecosystem services [65].

For example, a decrease in available irrigation flows in the study zone [48] would lead to the substitution of irrigation crops for other rain-fed crops. In this case, the values of the spectral indices (NDVI and NDWI) are modified, while the plot altitudes remain invariant.

The values of both indices for the most representative rain-fed crops in the area (almond, herbaceous crops, and grassland) were obtained by remote sensing for plots close to these crops on the reference date. From these, the LST was predicted for the 216 plots in the sample, assuming that plots were occupied by each of these crops. This gave the results shown in Table 5, where the average value predicted by the model for the current situation of irrigated citrus is also included.

Table 5. Predictions of LST for irrigated and rain-fed land.

Crops	NDVI (−1, 1)	NDWI (−1, 1)	LST Predicted (°C)	Dif. MEAN Citrus vs. Dry Land (*p*-Value)
Citrus	0.342	0.065	32.425	-
Almond	0.180	−0.033	33.624	1.199 (0.000)
Herbaceous	0.169	−0.039	33.649	1.224 (0.000)
Grassland	0.187	−0.044	33.642	1.217 (0.000)

The difference in mean temperature was significantly higher for rain-fed crops, with respect to the reference of irrigated citrus. The average increase ranged from 1.20 °C to 1.22 °C, which indicates an increase in LST close to 4%.

4. Discussion

In this paper, the ICE of citrus cultivation was determined using multiple linear regression models. It was confirmed, using Moran´s I index, that the estimates made using OLS were not appropriate, given the spatial dependence of the observations. The use of the GWR technique, after the selection of appropriate factors, seems appropriate to eliminate the spatial dependence bias. The GWR gave a model with a better fit to the observations. Thereby, GWR models yielded significantly better predictions of the LST than OLS models, in agreement with the results of other studies [29,40,44,67,68] which used local models to explain the LST variable.

Thus, in the study of the ICE phenomenon, it has been observed that OLS models do not accurately identify the spatial variation in the LST in a heterogeneous agricultural environment, such as the one studied here. Compared to these conventional regressions, GWR models have the potential to allow for a better understanding of the ICE and the associated factors. Thereby, the spatial variation for each of the citrus plots considered (Figure 3a) could be visualized, with a better explanation of the reduction in the LST (higher local R^2) in plots close to the coast, and with a trend for the LST to decrease in a NE–SW direction. Likewise, the three factors found to influence the ICE differed in their behaviors among the plots. The intensity of temperature reduction was greater in the NE sector of this agricultural zone, when the NDVI was taken into account (Figure 3c), and in the central-eastern part considering the NDWI (Figure 3d). In terms of altitude (Figure 3e), a greater increase in the LST was observed in central areas. Thus, greater vegetation cover and greater water content of the vegetation favor the provision of climate regulation ES.

The inverse relationship of the LST and NDVI shown in this study is consistent with the results of numerous papers [69,70], confirming the role of vegetation in the reduction of surface temperatures through the transfer of latent heat from the surface to the atmosphere by evapotranspiration.

In addition, the LST values showed an inverse relationship with the NDWI [71], demonstrating the importance of the water held in crops in reducing the surface temperature.

Regarding the third factor—the altitude of the plot—the result was, in principle, counter-intuitive, where higher elevation of a plot above sea level was associated with an increase in the LST. Nevertheless, given the special characteristics of the region, with low levels of altitude (most of the plots coincide with the coastal plain) and the proximity to the coast, this effect was expected. Moreover, given the low average altitude in the area, there have been other studies [41] that confirmed a direct relationship between elevation and the LST in low-altitude areas.

The effects of changes in land use and land cover on the ICE were determined. Differences of up to 1.22 °C between irrigated citrus crops and dry land in the study area were found. These differences in the LST were due to the different thermal capacity, roughness, and surface albedo that each type of land use has [69]. These differences (between irrigated and dry land) were in line with differences found in other studies: Yang et al. [34] showed that irrigation cooled daytime LST by 1.15 K in China, and Lemus-Canovas et al. [72] showed that green areas in cities can decrease the LST by up to 2.5 °C, compared to urban areas. Furthermore, Liu et al. [73] showed that irrigated rice fields experienced a temperature reduction of 1.85 K, compared to rain-fed maize fields.

In order to evaluate the relative importance of the ICE, a comparative study of the ICE and the rest of the ES and EDS present in this agroecosystem was conducted. Using the results of a recent study [8] which identified significant ES (climate regulation, crop productivity, and biodiversity) and EDS (groundwater pollution and water supply) in this same agroecosystem and study area, the trade-offs were calculated. When land-use changes from dry land to irrigated citrus crops happen, the climate regulation ES (reducing the LST by 1.22 °C) is not the only one affected. Such a land-use change would lead to an increase in agricultural productivity, with an average value of 23,000 €/ha, and a reduction in biodiversity by 40% of bird species in this area, in spite of an increase in the diversity of soil organisms. On the other hand, EDS would also be produced, such as water consumption, with values around of 6,000 m^3/ha and a groundwater pollution increase of 225 mg NO_3/L.

In this way, it is possible to consider the effects that restrictions on the availability of water in the area may have on the LST, given the scarcity of this resource [74]. Irrigation water restrictions would transform the current citrus plots into dry land, as well as altering the cold effect phenomenon and the rest of ES and EDS provided by the agroecosystem.

Although this change in surface temperature may seem small (3.62% cooling), it has great importance in arid and semi-arid areas such as Campo de Cartagena, given its influence on agricultural yields. Higher temperatures shorten the crop cycle and, consequently, alter the local climatic suitability for specific crops [75]. Likewise, as is well known in agroecosystems, the provision of shade and reduction of temperatures allows for higher water infiltration and retention rates, regulation of the air quality, reduction of greenhouse gas emissions, and a greater variety of ecological niches [76]. Therefore, variation in the LST has an impact on the activity and diversity of soil organisms [77], the avifauna [78], and biodiversity in general [75]. In addition, several studies [10,79] have shown that the ICE of crops can generate a higher bioclimatic quality, comfort zones, and a reduction in the use of heating appliances in cities, thus saving energy and contributing to a decrease in greenhouse gases.

Thus, the decrease of LST by more than 1 °C is a significant reduction, within the ES framework [14, 31,34,71–73,80,81]. This is an important value to provide climate regulation ES in irrigated lands. Climate regulation is a crucial service in the set of ES provided by agroecosystems [17]; especially so under an uncertain future where climate change [10] makes the development of effective mitigation and adaptation strategies even more important. This is evident in the priorities of the Common Agricultural Policy of the European Union, which are intended to promote local measures to preserve the ES of agricultural ecosystems.

5. Conclusions

In this paper, we evaluated the provisioning of climate regulation ES by agroecosystems—specifically, the ICE phenomenon—based on monitoring of the LST. To this end, a study considering the citrus crops in Campo de Cartagena, Southeastern Spain, was developed. Firstly, the existence of

the ICE was confirmed by means of LST variations. Then the factors that determine LST were studied using the GWR, improving the results of OLS. The GWR showed the influence of the NDVI, the NDWI, and the altitude in the generation of this climatic phenomenon, while a reduction of up to 1.22 ºC in the LST with respect to dry land was quantified. This reduction represents a 3.62% decrease in LST, with respect to dry land.

The factors that influence the ICE have provided new knowledge to develop local policies to improve the provision of climate regulation ES, which are fundamental in mitigating the effects of climate change—one of the most important socioeconomic challenges facing society. A practical implication of the results is to provide a quantitative way to take into account the LST in the design of agro-environmental schemes, in the same way that biodiversity protection or CO_2 storage are evaluated. Furthermore, it allows us to take into account seasonal crops planning for climate regulation ES. This is made possible by analyzing the conditions that can influence the service flow provided. These implications provide agricultural and policy planners and managers with a new vision in the provision of climate regulation ES through the design of citrus plots with abundant vegetation and water content.

This study is not exempt of limitations. The LST varies over time and only a fixed thermal image was used. Previous studies [30,82] showed differences in LST between days and seasons; however, some factors (such as NDVI) may not have an effect on the LST during night-time or in the winter season. Therefore, the results of this spatial analysis should be complemented by further studies that analyze the LST multitemporal effect. Moreover, a spatial comparison between different agricultural areas under different climatic conditions would be recommended.

On the other hand, a recent study [8] on this same agroecosystem and study area evaluated the synergies/trade-offs between agroecosystem ES, indicating the significance of climate regulation ES compared to other ES. Thus, the quantification of the ICE is a necessary step in the full evaluation of the agroecosystem ES. Land-use change from dry land to citrus crops resulted in a reduction in temperature; however, at the same time, it modifies other related ES, the most representative synergies being increases in the crop productivity (by 18,852 €/ha/°C) and water consumption (by 4918 m^3/ha/°C). Thus, socioeconomic benefits produced by the agricultural use of water are, therefore, broader than the traditional ones of food production or employment generation.

These results can be generalized to other semi-arid agricultural regions dedicated to irrigated citrus cultivation, as in the Spanish Levant or larger areas of the Mediterranean coast. This work establishes baseline values for the LST and its differences with other agricultural uses, in order to compare these results with other zones. Thus, this methodology constitutes an appropriate tool to complete the evaluation of agroecosystem ES, given that it allows the study and quantification of LST—one of the basic pillars (although less studied) of the climate regulation ES.

Author Contributions: Conceptualization, J.A.A.-G., F.A., and J.M.M.-P.; Methodology, J.A.A.-G., F.A., and J.M.M.-P.; Validation, J.A.A.-G.; Formal Analysis, J.A.A.-G.; Writing—Original Draft Preparation, J.A.A.-G.; Writing—Review & Editing, J.A.A.-G., F.A., and J.M.M.-P.; Visualization, J.A.A.-G., F.A., and J.M.M.-P.; Project Administration, J.M.M.-P., and F.A. All authors have read and agreed to the published version of the manuscript.

Funding: This research was funded by AGRISERVI project, grant number AGL2015-64411-R financed by "Spanish Ministry of Economics and Competitiveness (MINECO)", and the 20912/PI/18 project, financed by "Fundación Séneca-Agencia de Ciencia y Tecnología de la Región de Murcia". The authors are also grateful for the financing of the first author´s pre-doctoral research by the "Spanish Ministry of Education, Culture and Sport (MECD) (FPU16/03562)".

Conflicts of Interest: The authors declare no conflict of interest.

Appendix A

Table A1. Descriptive statistics on dependent and independent variables.

Variables	Mean	Standard Deviation	Minimum	Maximum
LST (°C)	32.470	1.533	28.540	36.090
NDVI (−1,1)	0.342	0.137	0.082	0.668
NDWI (−1,1)	0.065	0.088	−0.095	0.313
Dist-coast (km)	9.647	6.089	0.504	31.090
Altitude (m)	58.560	52.060	6.000	282.000
Slope (°)	1.497	2.311	0.000	12.140
Tair (°C)	25.875	0.383	24.880	26.624
Orientation (%)				
Shaded spot	7.43			
Flat	75.25			
Sunny spot	17.32			

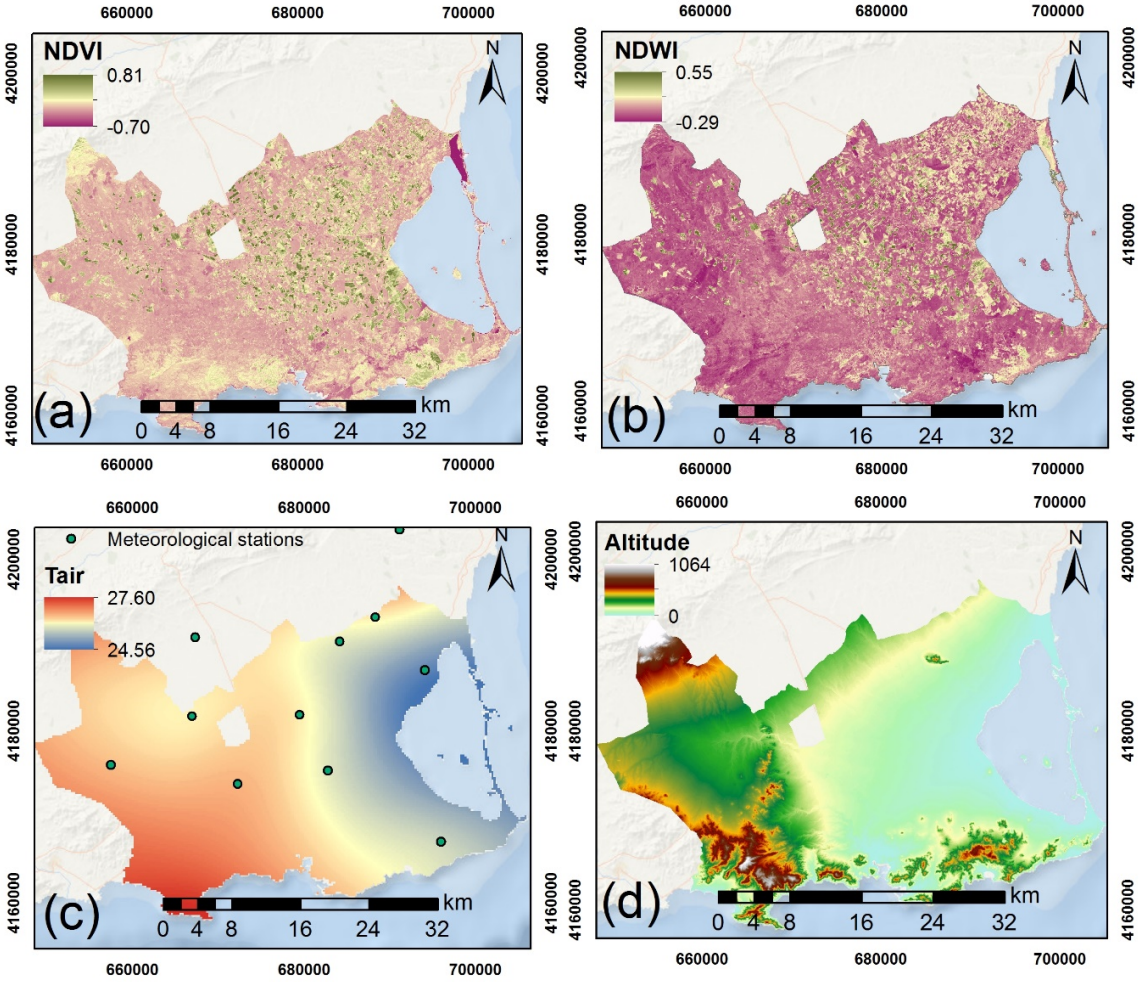

Figure A1. *Cont.*

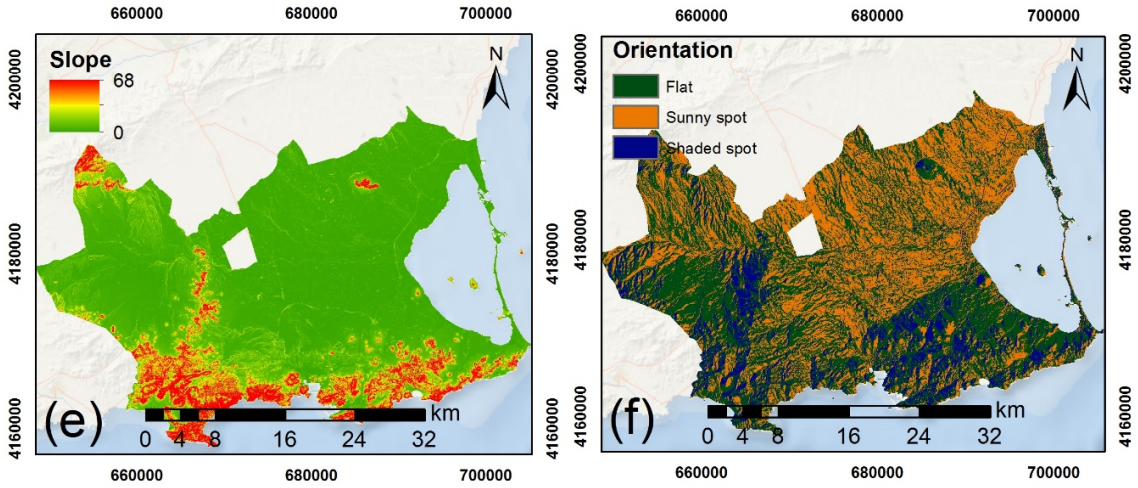

Figure A1. Spatial distribution of factors: NDVI (**a**), NDWI (**b**), Tair (**c**), Altitude (**d**), Slope (**e**), and Orientation (**f**).

References

1. Maes, J.; Liquete, C.; Teller, A.; Erhard, M.; Paracchini, M.L.; Barredo, J.I.; Grizzetti, B.; Cardoso, A.; Somma, F.; Petersen, J.-E.; et al. An indicator framework for assessing ecosystem services in support of the EU Biodiversity Strategy to 2020. *Ecosyst. Serv.* **2016**, *17*, 14–23. [CrossRef]
2. MEA. *Ecosystem and Human Well-being: Synthesis*; Island Press: Washington, DC, USA, 2005.
3. Shackleton, C.M.; Ruwanza, S.; Sanni, G.K.S.; Bennett, S.; De Lacy, P.; Modipa, R.; Mtati, N.; Sachikonye, M.; Thondhlana, G. Unpacking Pandora's Box: Understanding and categorising ecosystem disservices for environmental management and human wellbeing. *Ecosystems* **2016**, *19*, 587–600. [CrossRef]
4. Haines-Young, R.; Potschin, M. *Common International Classification of Ecosystem Services (CICES, Version 4.1)*; European Environment Agency: Nottingham, UK, 2012.
5. Waldman, K.B.; Attari, S.Z.; Gower, D.B.; Giroux, S.A.; Caylor, K.K.; Evans, T.P. The salience of climate change in farmer decision-making within smallholder semi-arid agroecosystems. *Climatic Change* **2019**, *156*, 527–543. [CrossRef]
6. Alcon, F.; Marín-Miñano, C.; Zabala, J.A.; de-Miguel, M.D.; Martínez-Paz, J.M. Valuing diversification benefits through intercropping in Mediterranean agroecosystems: A choice experiment approach. *Ecol. Econ.* **2020**, *171*, 106593. [CrossRef]
7. Castelli, G.; Castelli, F.; Bresci, E. Mesoclimate regulation induced by landscape restoration and water harvesting in agroecosystems of the horn of Africa. *Agric. Ecosyst. Environ.* **2019**, *275*, 54–64. [CrossRef]
8. Zabala, J.A.; Marín-Miñano, C.; Albaladejo-García, J.A.; López-Becerra, E.I.; de Miguel, M.D.; Martínez-Paz, J.M.; Alcon, F. A Valuation-Based Approach for Irrigated Agroecosystem Services. In Proceedings of the European Association of Agricultural Economics Seminar, Brussels, Belgium, 28–29 May 2019; p. 12.
9. Smith, P.; Ashmore, M.R.; Black, H.I.J.; Burgess, P.J.; Evans, C.D.; Quine, T.A.; Thomson, A.M.; Hicks, K.; Orr, H.G. The role of ecosystems and their management in regulating climate, and soil, water and air quality. *J. Appl. Ecol.* **2013**, *50*, 812–829. [CrossRef]
10. Locatelli, B. Ecosystem Services and Climate Change. In *Routledge Handbook of Ecosystem Services*; Potschin, R., Haines-Young, R., Fish, R., Turner, R.K., Eds.; Routledge: New York, NY, USA, 2016; pp. 481–490.
11. Lobell, D.B.; Bonfils, C.J.; Kueppers, L.M.; Snyder, M.A. Irrigation cooling effect on temperature and heat index extremes. *Geophys. Res. Lett.* **2008**, *35*, L09705. [CrossRef]
12. Xu, L.; Shi, Z.; Wang, Y.; Chu, X.; Yu, P.; Xiong, W.; Zuo, H.; Zhang, S. Agricultural irrigation-induced climatic effects: A case study in the middle and southern Loess Plateau area, China. *Int. J. Climatol.* **2017**, *37*, 2620–2632. [CrossRef]
13. Bonfils, C.; Lobell, D. Empirical evidence for a recent slowdown in irrigation-induced cooling. *Proc. Natl. Acad. Sci. USA* **2007**, *104*, 13582–13587. [CrossRef]

14. Estoque, R.C.; Murayama, Y.; Myint, S.W. Effects of landscape composition and pattern on land surface temperature: An urban heat island study in the megacities of Southeast Asia. *Sci. Total Environ.* **2017**, *577*, 349–359. [CrossRef]
15. Duveiller, G.; Hooker, J.; Cescatti, A. The mark of vegetation change on Earth's surface energy balance. *Nat. Commun.* **2018**, *9*, 679. [CrossRef] [PubMed]
16. Crossman, N.D.; Burkhard, B.; Nedkov, S.; Willemen, L.; Petz, K.; Palomo, I.; Drakou, E.G.; Martin-Lopez, B.; McPhearson, T.; Boyanova, K.; et al. A blueprint for mapping and modelling ecosystem services. *Ecosyst. Serv.* **2013**, *4*, 4–14. [CrossRef]
17. Blanco-Canqui, H.; Shaver, T.M.; Lindquist, J.L.; Shapiro, C.A.; Elmore, R.W.; Francis, C.A.; Hergert, G.W. Cover crops and ecosystem services: Insights from studies in temperate soils. *Agron. J.* **2015**, *107*, 2449–2474. [CrossRef]
18. Hodge, I.; Hauck, J.; Bonn, A. The alignment of agricultural and nature conservation policies in the European Union. *Conserv. Biol.* **2015**, *29*, 996–1005. [CrossRef]
19. Yu, Z.; Guo, X.; Jørgensen, G.; Vejre, H. How can urban green spaces be planned for climate adaptation in subtropical cities? *Ecol. Indic.* **2017**, *82*, 152–162. [CrossRef]
20. Li, W.; Cao, Q.; Lang, K.; Wu, J. Linking potential heat source and sink to urban heat island: Heterogeneous effects of landscape pattern on land surface temperature. *Sci. Total Environ.* **2017**, *586*, 457–465. [CrossRef]
21. Hamada, S.; Tanaka, T.; Ohta, T. Impacts of land use and topography on the cooling effect of green areas on surrounding urban areas. *Urban For. Urban Green.* **2013**, *12*, 426–434. [CrossRef]
22. Zardo, L.; Geneletti, D.; Pérez-Soba, M.; Van Eupen, M. Estimating the cooling capacity of green infrastructures to support urban planning. *Ecosyst. Serv.* **2017**, *26*, 225–235. [CrossRef]
23. Li, X.; Zhou, W.; Ouyang, Z. Relationship between land surface temperature and spatial pattern of greenspace: What are the effects of spatial resolution? *Landsc. Urban Plann.* **2013**, *114*, 1–8.
24. Kumar, R.; Mishra, V.; Buzan, J.; Kumar, R.; Shindell, D.; Huber, M. Dominant control of agriculture and irrigation on urban heat island in India. *Sci. Rep.* **2017**, *7*, 14054. [CrossRef]
25. Cook, B.I.; Puma, M.J.; Krakauer, N.Y. Irrigation induced surface cooling in the context of modern and increased greenhouse gas forcing. *Clim. Dyn.* **2011**, *37*, 1587–1600.
26. Thiery, W.; Davin, E.L.; Lawrence, D.M.; Hirsch, A.L.; Hauser, M.; Seneviratne, S.I. Present-day irrigation mitigates heat extremes. *J. Geophys. Res. Atmosph.* **2017**, *122*, 1403–1422. [CrossRef]
27. Thiery, W.; Visser, A.J.; Fischer, E.M.; Hauser, M.; Hirsch, A.L.; Lawrence, D.M.; Seneviratne, S.I. Warming of hot extremes alleviated by expanding irrigation. *Local Cool. Warm.* **2020**, *11*, 1–7. [CrossRef] [PubMed]
28. Guimberteau, M.; Laval, K.; Perrier, A.; Polcher, J. Global effect of irrigation and its impact on the onset of the Indian summer monsoon. *Clim. Dyn.* **2012**, *39*, 1329–1348.
29. Shaker RRAltman, Y.; Deng, C.; Vaz, E.; Forsythe, K.W. Investigating urban heat island through spatial analysis of New York City streetscapes. *J. Clean. Prod.* **2019**, *233*, 972–992. [CrossRef]
30. Kang, S.; Eltahir, E.A. Impact of irrigation on regional climate over Eastern China. *Geophys. Res. Lett.* **2019**, *46*, 5499–5505. [CrossRef]
31. Zhu, X.; Liang, S.; Pan, Y. Observational evidence of the cooling effect of agricultural irrigation in Jilin, China. *Clim. Chang.* **2012**, *114*, 799–811. [CrossRef]
32. Reyes, B.; Hogue, T.; Maxwell, R. Urban irrigation suppresses land surface temperature and changes the hydrologic regime in semi-arid regions. *Water* **2018**, *10*, 1563. [CrossRef]
33. Wang, X.; Guo, W.; Qiu, B.; Liu, Y.; Sun, J.; Ding, A. Quantifying the contribution of land use change to surface temperature in the lower reaches of the Yangtze River. *Atmosph. Chem. Phys.* **2017**, *17*, 4989–4996. [CrossRef]
34. Yang, Q.; Huang, X.; Tang, Q. Irrigation cooling effect on land surface temperature across China based on satellite observations. *Sci. Total Environ.* **2020**, *705*, 135984. [CrossRef]
35. Vlassova, L.; Tufiño, P.R.; Llovería, R.M. Variabilidad espacio-temporal de la temperatura de superficie en ecosistemas de dehesa estimada mediante imágenes Landsat TM: El papel del arbolado. *Geographicalia* **2016**, *68*, 69–86. [CrossRef]
36. Karnieli, A.; Agam, N.; Pinker, R.; Anderson, M.; Imhoff, M.L.; Gutman, G.G.; Panov, N.; Goldberg, A. Use of NDVI and land surface temperature for drought assessment: Merits and limitations. *J. Clim.* **2010**, *23*, 618–633.
37. Anselin, L. *Spatial Econometrics: Methods and Models*; Springer: Dordrecht, The Netherlands, 1988.

38. Acharya, B.K.; Cao, C.; Lakes, T.; Chen, W.; Naeem, S.; Pandit, S. Modeling the spatially varying risk factors of dengue fever in Jhapa district, Nepal, using the semi-parametric geographically weighted regression model. *Int. J. Biometeorol.* **2018**, *62*, 1973–1986. [PubMed]
39. Arabameri, A.; Pradhan, B.; Rezaei, K. Gully erosion zonation mapping using integrated geographically weighted regression with certainty factor and random forest models in GIS. *J. Environ. Manag.* **2019**, *232*, 928–942.
40. Zhao, C.; Jensen, J.; Weng, Q.; Weaver, R. A Geographically Weighted Regression Analysis of the Underlying Factors Related to the Surface Urban Heat Island Phenomenon. *Remote Sens.* **2018**, *10*, 1428.
41. Ivajnšič, D.; Kaligarič, M.; Žiberna, I. Geographically weighted regression of the urban heat island of a small city. *Appl. Geogr.* **2014**, *53*, 341–353. [CrossRef]
42. Tian, F.; Qiu, Y.G.; Yang, Y.H.; Xiong, Y.J.; Wang, P. Studies on the relationships between land surface temperature and environmental factors in an inland river catchment based on geographically weighted regression and MODIS data. *IEEE J. Sel. Top. Appl. Earth Obs. Remote Sens.* **2012**, *5*, 687–698. [CrossRef]
43. Zhou, X.; Wang, Y.C. Dynamics of Land Surface Temperature in Response to Land-Use/Cover Change. *Geogr. Res.* **2011**, *49*, 23–36. [CrossRef]
44. Yin, C.; Yuan, M.; Lu, Y.; Huang, Y.; Liu, Y. Effects of urban form on the urban heat island effect based on spatial regression model. *Sci. Total Environ.* **2018**, *634*, 696–704. [CrossRef]
45. Malek, Ž.; Verburg, P.H. Adaptation of land management in the Mediterranean under scenarios of irrigation water use and availability. *Mitig. Adapt. Strateg. Glob. Chang.* **2018**, *23*, 821–837.
46. Volk, M.I.; Hoctor, T.S.; Nettles, B.B.; Hilsenbeck, R.; Putz, F.E.; Oetting, J. Florida Land Use and Land Cover Change in the Past 100 Years. In *Florida's Climate: Changes, Variations, & Impacts*; Chassignet, E.P., Jones, J.W., Misra, V., Obeysekera, J., Eds.; Florida Climate Institute: Gainesville, FL, USA, 2017; pp. 51–82.
47. Roberts, D.A.; Dennison, P.E.; Roth, K.L.; Dudley, K.; Hulley, G. Relationships between dominant plant species, fractional cover and land surface temperature in a Mediterranean ecosystem. *Remote Sens. Environ.* **2015**, *167*, 152–167. [CrossRef]
48. Pellicer-Martínez, F.; Martínez-Paz, J.M. Probabilistic evaluation of the water footprint of a river basin: Accounting method and case study in the Segura River Basin, Spain. *Sci. Total Environ.* **2018**, *627*, 28–38. [CrossRef] [PubMed]
49. Alcon, F.; Tapsuwan, S.; Martínez-Paz, J.-M.; Brouwer, R.; de Miguel, M.D. Forecasting deficit irrigation adoption using a mixed stakeholder assessment methodology. *Technol. Forecast. Soc. Chang.* **2014**, *83*, 183–193. [CrossRef]
50. CREM. Censo Agrario. Available online: http://econet.carm.es/web/crem/inicio//crem/sicrem/PU590/Indice1 (accessed on 28 January 2019).
51. SIOSE. Sistema de Información Sobre la Ocupación del Suelo en España. Available online: https://www.siose.es/web/guest/base-de-datos (accessed on 23 January 2019).
52. Liou, Y.A.; Nguyen, A.K.; Li, M.H. Assessing spatiotemporal eco-environmental vulnerability by Landsat data. *Ecol. Indic.* **2017**, *80*, 52–65. [CrossRef]
53. Godinho, S.; Gil, A.; Guiomar, N.; Costa, M.J.; Neves, N. Assessing the role of Mediterranean evergreen oaks canopy cover in land surface albedo and temperature using a remote sensing-based approach. *Appl. Geogr.* **2016**, *74*, 84–94. [CrossRef]
54. Sekertekin, A.; Bonafoni, S. Land Surface Temperature Retrieval from Landsat 5, 7, and 8 over Rural Areas: Assessment of Different Retrieval Algorithms and Emissivity Models and Toolbox Implementation. *Remote Sens.* **2020**, *12*, 294. [CrossRef]
55. Kong, F.; Yin, H.; Wang, C.; Cavan, G.; James, P. A satellite image-based analysis of factors contributing to the green-space cool island intensity on a city scale. *Urban For. Urban Green.* **2014**, *13*, 846–853. [CrossRef]
56. Chander, G.; Markham, B. Revised Landsat-5 TM radiometric calibration procedures and postcalibration dynamic ranges. *IEEE Trans. Geosci. Remote Sens.* **2003**, *41*, 2674–2677. [CrossRef]
57. USGS. Landsat 8 Conversion to Radiance, Reflectance and At-Satellite Brightness Temperature Using the USGS Landsat 8 Product. Available online: https://landsat.usgs.gov/using-usgs-landsat-8-product (accessed on 28 May 2020).
58. Sobrino, J.A.; Jimenez-Munoz, J.C.; Paolini, L. Land surface temperature retrieval from LANDSAT TM 5. *Remote Sens. Environ.* **2004**, *90*, 434–440. [CrossRef]

59. Zheng, H.; Lin, H.; Zhu, X. Spatiotemporal Patterns of Terrestrial Evapotranspiration in Response to Climate and Vegetation Coverage Changes across the Chinese Loess Plateau. *Water* **2019**, *11*, 1625. [CrossRef]
60. SIAM. Sistema de Información Agrario de Murcia. *Informe Agrometeorológico.* Available online: http://siam.imida.es/apex/f?p=101:1:1753201960247786 (accessed on 20 January 2019).
61. CNIG. Centro Nacional de Información Geográfica. *Modelos Digitales de Elevaciones and SIOSE.* Available online: http://centrodedescargas.cnig.es/CentroDescargas/index.jsp (accessed on 25 January 2019).
62. Martínez-Paz, J.M. Irrigation cooling effect of citrus cultivation in Campo de Cartagena (Murcia, Spain). *PANGAEA* **2019**. [CrossRef]
63. Fotheringham, A.S.; Brunsdon, C.; Charlton, M. *Geographically Weighted Regression: The analysis of Spatially Varying Relationships*; John Wiley & Sons: Hoboken, NJ, USA, 2003.
64. Hadayeghi, A.; Shalaby, A.S.; Persaud, B.N. Development of planning level transportation safety tools using Geographically Weighted Poisson Regression. *Accid. Analys. Prev.* **2010**, *42*, 676–688. [CrossRef] [PubMed]
65. Gutiérrez-Puebla, J.; García-Palomares, J.; Daniel-Cardozo, O. Regresión Geográficamente Ponderada (GWR) y estimación de la demanda de las estaciones del Metro de Madrid. In Proceedings of the XV Congreso Nacional de Tecnologías de la Información Geográfica, Madrid, Spain, 19–21 September 2012; pp. 19–21.
66. Greene, W.H. *Econometric Analysis*; Prentice Hall: Upper Saddle River, NJ, USA, 1997.
67. Alibakhshi, Z.; Ahmadi, M.; Asl, M.F. Modeling Biophysical Variables and Land Surface Temperature Using the GWR Model: Case Study—Tehran and Its Satellite Cities. *J. Indian Soc. Remote Sens.* **2020**, *48*, 59–70. [CrossRef]
68. Hu, X.; Xu, H. Spatial variability of urban climate in response to quantitative trait of land cover based on GWR model. *Environ. Monit. Assess.* **2019**, *191*, 194. [CrossRef]
69. Deng, Y.; Wang, S.; Bai, X.; Tian, Y.; Wu, L.; Xiao, J.; Chen, F.; Qian, Q. Relationship among land surface temperature and LUCC, NDVI in typical karst area. *Sci. Rep.* **2018**, *8*, 641. [CrossRef]
70. Yuan, X.; Wang, W.; Cui, J.; Meng, F.; Kurban, A.; De Maeyer, P. Vegetation changes and land surface feedbacks drive shifts in local temperatures over Central Asia. *Sci. Rep.* **2017**, *7*, 3287. [CrossRef]
71. Serrano, S.; Marques Da Silva, J. Evaluation of normalized difference water index as a tool for monitoring pasture seasonal and inter-annual variability in a Mediterranean agro-silvo-pastoral system. *Water* **2019**, *11*, 62. [CrossRef]
72. Lemus-Canovas, M.; Martin-Vide, J.; Moreno-Garcia, M.C.; Lopez-Bustins, J.A. Estimating Barcelona's metropolitan daytime hot and cold poles using Landsat-8 Land Surface Temperature. *Sci. Total Environ.* **2020**, *699*, 134307. [CrossRef]
73. Liu, T.; Yu, L.; Zhang, S. Land surface temperature response to irrigated paddy field expansion: A case study of semi-arid western Jilin Province, China. *Sci. Rep.* **2019**, *9*, 1–8.
74. Perni, A.; Martínez-Paz, J.M. A participatory approach for selecting cost-effective measures in the WFD context: The Mar Menor (SE Spain). *Sci. Total Environ.* **2013**, *458*, 303–311. [CrossRef]
75. Calzadilla, A.; Rehdanz, K.; Betts, R.; Falloon, P.; Wiltshire, A.; Tol, R.S.J. Climate change impacts on global agriculture. *Clim. Chang.* **2013**, *120*, 357–374. [CrossRef]
76. EC. *Soil Biodiversity: Functions, Threats and Tools for Policy Makers*. DG Environment, European Communities. 2010. Available online: https://ec.europa.eu/environment/archives/soil/pdf/biodiversity_report.pdf (accessed on 14 May 2018).
77. Schaefer, H.C.; Jetz, W.; Böhning-Gaese, K. Impact of climate change on migratory birds: Community reassembly versus adaptation. *Glob. Ecol. Biogeogr.* **2008**, *17*, 38–49. [CrossRef]
78. Scarano, F.R. Biodiversity Sector: Risks of Temperature Increase to Biodiversity and Ecosystems. In *Climate Change Risks in Brazil*; Marengo, J.A., Nobre, C.A., Soares, W.R., Eds.; Springer: Cham, Switzerland, 2019; pp. 131–141.
79. Zhou, D.; Li, D.; Sun, G.; Zhang, L.; Liu, Y.; Hao, L. Contrasting effects of urbanization and agriculture on surface temperature in eastern China. *J. Geophys. Res. Atmosph.* **2016**, *121*, 9597–9606. [CrossRef]
80. Heatlandlife. Available online: https://heatlandlife.eu/el-proyecto-life-heatland-prueba-en-murcia-un-asfalto-frio-que-reduce-la-contaminacion-en-las-ciudades/ (accessed on 30 January 2018).

81. Li, Y.; Zhao, M.; Motesharrei, S.; Mu, Q.; Kalnay, E.; Li, S. Local cooling and warming effects of forests based on satellite observations. *Nat. Comm.* **2015**, *6*, 6603.
82. Yuan, F.; Bauer, M.E. Comparison of impervious surface area and normalized difference vegetation index as indicators of surface urban heat island effects in Landsat imagery. *Remote Sens. Environ.* **2007**, *106*, 375–386. [CrossRef]